*The 2013 World Congress on*
***Advances in Nano, Biomechanics, Robotics, and Energy Research (ANBRE13)***
*Seoul, Korea, August 25-28, 2013*

# Preparation of Ag-Nanoparticle-Loaded $MnO_2$ Nanosheets and Their Capacitance Behavior

Gaini Zhang, Lu Zheng, Miao Zhang, Shaohua Guo, Zong-Huai Liu*, Zupei Yang, and Zenglin Wang

*School of Materials Science and Engineering, Shaanxi Normal University, Xi'an 710062, PR China*
*1)zhliu@snnu.deu.cn*

## ABSTRACT

Manganese oxide has a potential application as electrode material of electrochemical capacitor because of abundant resource, low cost, environment compatibility and high theoretical capacitance. However, the poor conductivity of the $MnO_2$ is a major problem in the electrochemical application. We prepared Ag/$MnO_2$ compound by a reassembling reaction between $Ag^+$ ions and delaminated manganese oxide nanosheets, followed by a reduction treatment. The addition of silver nanoparticles optimized the conductivity of the material and prevented the reassembling process of the manganese oxide nanosheets. The Ag/$MnO_2$ electrode shows a characteristic Faradic capacitance behavior. It is a promising electrode for an energy storage/conversion device with excellent performance.

## 1. INTRODUCTION

In recent years, the electrochemical capacitors have received considerable attention because of their high capacity, high power density and long cycle life.[1] The research results show that the good performance of electrochemical capacitors usually results from the high specific surface area as well as the high reversible redox reactions of the electrode materials.[2] Porous carbon materials, conducting polymers and transition metal oxides are fundamental candidates for the electrochemical electrode materials.[3] Among the transition metal oxides with various valence states, manganese oxide is one of the most promising pseudocapacitor electrode materials because of its high specific capacitance, environmental compatibility and cost effectiveness.[4,5] Up to now, manganese oxide has been deeply studied to attain more information about its intrinsic property and find the relation between morphological, structural and compositional characteristics of material with the electrochemical performance.[6–8]

The specific surface area and the reversible redox reaction of electrode materials have an obvious influence on the performance of electrochemical capacitors.[9] The large specific surface area and high electrical conductivity can improve the capacitance performance of the electrode materials. The bulk manganese oxides have a small specific surface area and low electrical conductivity because of their semiconducting

* To whom correspondence should be addressed. Tel: 86-29-81530706 Fax: 86-29-81530702

character, which seriously limit their application as the electrode materials of electrochemical capacitors.[10,11] Therefore, manganese oxide hybrid materials with a large specific surface area and high electrical conductivity are expected. In general, the electrical conductivity of the $MnO_2$-based materials can be improved by doping some conductive materials into manganese oxides.

Manganese oxide nanosheets have not only distinctive physicochemical properties, associated with dimensions in the nanometer scope, but also a large specific surface area. They can be obtained through the delamination reaction of the layered $MnO_2$, and can be employed as a new class of nanoscale materials.[12] Sophisticated functionalities or nanodevices may be designed through the selection of nanosheets and combining materials, and precise control over their arrangement at the molecular scale.[13,14] Because of the excellent electronic conductivity of silver, it would be an ideal conductor to form electron−transferring channels during manganese dioxide discharging. Recent investigations show that the battery performance of the lithium manganese dioxide electrode can be significantly improved by doping 1-8 wt % Ag.[15] For example, in comparison to pure $RuO_2$, Ag-doped $RuO_2$ shows much higher specific capacitance because of the increase in conductivity.[16] Therefore, Ag-doped $MnO_2$ is expected to increase the conductivity and shows higher specific capacitance. Up to now, Ag-doped $MnO_2$ films have been prepared by a cathodic electrolytic deposition from the $KMnO_4$ aqueous solution containing $AgNO_3$.[17] The prepared films show improved capacitive behavior and lower resistance compared to pure $MnO_2$ films, but the preparation method has a complex procedure and high cost. Silver decorated γ-manganese dioxide nanorods are obtained evenly by a wet impregnation method, and the utility efficiency of the as-prepared material is greatly enhanced when silver particles are introduction. Silver nanoparticles not only accelerate the electron conducting but also improve the proton diffusion throughout the electrode.[18] Moreover, $Ag_2O$ can be used as electrode materials in silver oxide batteries. Because of the high energy density, the silver oxide battery is an ideal electronic device for use in small, thin button batteries. As the cathode continues to discharge, the silver metal produced by the reaction helps to keep the internal cell resistance low and the closed-circuit voltage high.[19–21] In the present work, Ag-loaded manganese oxide nanosheets are prepared by a reassembling reaction between $Ag^+$ ions and delaminated manganese oxide nanosheets and followed by a reduction process. This design takes not only full advantage of the pseudocapacitance from manganese oxide, but also the high electrical conductivity of silver.

## 2. Experimental Section

### 2.1. Material

Tetramethylammonium hydroxide (25 wt %) was purchased from Alfa Aesar Co., and poly(N-vinylpyrrolidone), $Mn(NO_3)_2$ (50%), $H_2O_2$ (30%), $HNO_3$(65%), NaOH, $AgNO_3$, $Na_2SO_4$ and ethanol were analytical grade without further purification. Deionized water was used throughout the experiments.

### 2.2. Synthesis of the Ag-$MnO_2$ material

The starting material, proton-type birnessite manganese oxide (H-BirMO) was synthesized and delaminated by the method described previously.[22,23] H-BirMO (0.5 g)

was treated in a 0.35 mol $L^{-1}$, 125 mL aqueous solution of tetramethylammonium hydroxide (TMAOH) for 7 days at room temperature. The amount of TMAOH added were 25–fold that of the exchangeable capacity of H-BirMO. After soaking, the colloidal suspension was centrifuged at a speed of 13000 rpm for 20 min and washed with deionized water to obtain delaminated BirMO slurry, which contained well dispersed manganese oxide nanosheets. Then 0.1 mol $L^{-1}$ $AgNO_3$ aqueous solution was added into the delaminated BirMO slurry, and the suspension was stirred for 24 h at room temperature. The obtained sediment was filtered, washed with deionized water, and dried at room temperature for 24 h, $Ag_2O$ nanoparticles-loaded manganese oxide nanosheets were obtained, which was abbreviated as $Ag_2O$-$MnO_2$. Sample $Ag_2O$-$MnO_2$ was then added into a mixture solution of PVP (0.1 g) and ethanol (100 mL), and the mixture was refluxed at 70 °C for 6 h while stirring in a thermostatic oil bath and followed by naturally cooling to room temperature. The obtained sediment was filtered, washed with ethanol and dried at room temperature for 24 h, Ag loaded-manganese oxide nanosheets were obtained, which was abbreviated as Ag-$MnO_2$.

2.3. Structure Characterization

The X-ray diffraction (XRD) analysis was performed on a D/Max-3c X-ray diffractometer with Cu K$\alpha$ radiation ($\lambda$=1.5406 Å) scanning from 5° to 70°, using an operation voltage and current of 40 kV and 30 mA, respectively. Transmission electron microscope (TEM) images were collected using a JEM-2100 microscope working at 120 kV. X-ray photoelectron spectroscopy (XPS) was performed with a K-Alpha spectrometer using Al K$\alpha$ radiation (1486.6 eV) at a power of 150 W (accelerating voltage at 12 kV and current at 6 mA) in a vacuum of $8.0\times10^{-8}$ mPa. To ensure the accuracy of the data measured, all the binding energies were calibrated relative to the C1s peak (284.6 eV) from hydrocarbons adsorbed on the surface of the samples.[24] The Ag content was determined by atomic absorption spectroscopy after dissolving a weighed amount of Ag-$MnO_2$ material in a mixed solution of $HNO_3$ and $H_2O_2$.

2.4. Electrochemical Measurement

The working electrode was prepared by mixing active materials ($MnO_2$, $Ag_2O$-$MnO_2$, or Ag-$MnO_2$) (75 wt %), acetylene black (20 wt %) and polyvinylidene fluoride (5 wt %) (the purity of acetylene black and polyvinylidene fluoride are battery grade). The two former constituents were first mixed together to obtain a homogeneous black power. The polyvinylidene fluoride solution (0.02 g $mL^{-1}$, in N-methyl-ketopyrrolidine) was added. This resulted in a rubber-like paste, it was then brush-coated onto a Ni foam current collector with a definite area of 2.0 $cm^2$. The foam was dried at 110 °C in air for 12 h for removal of the solvent, and it was uniaxially pressed to make the electrode material completely adhere to the current collector.

Cyclic voltammetry (CV) and electrochemical impedance spectroscopy (EIS) were measured using a typical three-electrode system. A CS350 electrochemical workstation (CorrTest Instrument Co., Wuhan, China) was used for the electrochemical measurement. A beaker type electrochemical cell was equipped with a $MnO_2$ based working electrode, a Pt-foil (2 $cm^2$) as the counter electrode and saturated calomel electrode (SCE) as the reference electrode. CV curves were preformed between -0.05 and 0.95 V in 1 mol $L^{-1}$ $Na_2SO_4$ electrolyte. The average specific capacitance (SC) was evaluated according to the following equations:[25]

$$i = \left( \int_{Va}^{Vc} i(v)\, dv \right) \Big/ (Vc - Va)$$

$$C_{\mathrm{m}} = i / mv$$

Where m is the mass of the active material impregnated into nickel foam, not including the weight of the additives in the electrode; v is the potential scanning rate; i is the even current response, which is obtained through integrating the area of the curves; Va and Vc represent the lowest and highest voltage, respectively. EIS was measured in the frequency ranges from 0.5 Hz to $8\times10^4$ Hz.

## 3. RESULTS AND DISCUSSION

### 3.1. Material Characterization

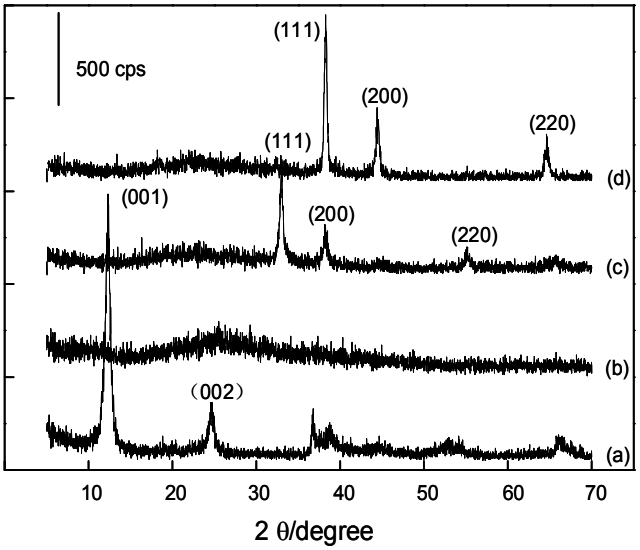


Fig.1 XRD patterns of samples obtained at different stages: H-BirMO (a), delaminated $MnO_2$ slurry (b), $Ag_2O$-$MnO_2$ (c), and Ag-$MnO_2$ material (d).

The XRD patterns of the samples obtained at different stages are shown in Figure 1. Precursor H-BirMO shows two obvious diffraction peaks at around 12.3° (001 planes) and 24.6° (002 planes), suggesting that the prepared H-BirMO belongs to δ-type crystal with a layered structure and a basal spacing of 0.73 nm, with crystal water and exchangeable $H^+$ ions in the interlayer space (Fig.1a).[26] The precursor H-BirMO was soaked in 0.35 mol $L^{-1}$ TMAOH solution for 7 days and then washed with distilled water. The obtained BirMO slurry gives no clear peaks but only an amorphous halo (Fig. 1b). The halo can be interpreted as scattering from the nanosheets which are aggregated irregularly, similar to the case of layered titanic acid or graphite oxide.[27,28] This indicates that the water washing causes the delamination of stacked layered manganese oxide plates to the individual primary plates.[29] For $Ag_2O$-$MnO_2$ material, the representative diffraction peaks can be indexed to silver oxide, which are agree well with the value in the standard card [Joint Committee on Powder Diffraction Standard (JCPDS) 65-3289), and no characteristic peaks of manganese oxide are observed (Fig. 1c). These results

suggest that the restacking process of the manganese oxide nanosheets is effectively prevented, and manganese oxide nanosheets exist in a complete exfoliation state in $Ag_2O$-$MnO_2$ material. Although there is no report on the preparation of $Ag_2O$-loaded $MnO_2$ material by a delamination/reassembling process, similar research results can be observed from the preparation of metal oxide modified graphite. In these research works,[30,31] the diffraction peaks of graphite nanosheets become weak or even disappear if the regular stacks of graphite nanosheets are destroyed by exfoliation. For Ag-$MnO_2$ material, the three strong diffraction peaks located at about 38.1º, 44.3º and 64.4º can be indexed as the (111), (200) and (220) planes of metal Ag (Fig. 1d), respectively, which are consistent with the face-centered cubic structure of Ag in JCPDS No. 65-2871. According to the atomic absorption spectroscopy experimental

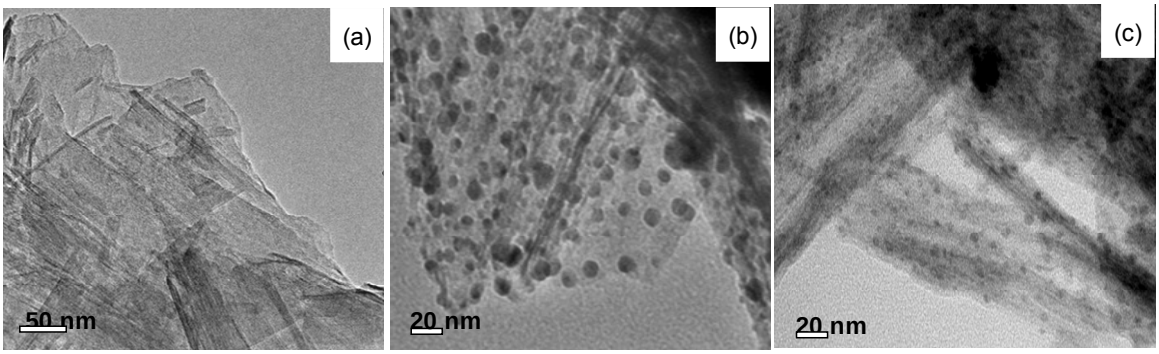


result, the Ag content is 34.93%.

Fig.2 TEM images of $MnO_2$ nanosheets (a), $Ag_2O$-$MnO_2$ (b), and Ag-$MnO_2$ materials (c).

TEM photographs of $MnO_2$ nanosheets, $Ag_2O$-$MnO_2$ and Ag-$MnO_2$ materials are similar to each other and mainly consist of platelike $MnO_2$ (Fig. 2). For the delaminated BirMO slurry, thin transparent platelets of width less than 0.5 μm are easily observed, which are comparable to the crystal dimensions of the precursor H-BirMO (Fig. 2a). The submicrometers to micrometer-sized nanosheets are contrasting to the nanosized manganese oxide with lateral dimensions below 50 nm that has been derived by delamination of H-BirMO.[32] TEM results indicate that the delamination process has occurred at the layer level without destroying the nanosheets. The delaminated BirMO slurry is dropped into $AgNO_3$ solution. The obtained $Ag_2O$-$MnO_2$ material still maintains the thin transparent platelet morphology. $Ag_2O$ nanoparticles with a size distribution from about 5 to 15 nm are distributed homogenously on the $MnO_2$ nanosheets (Fig. 2b), suggesting that $MnO_2$ nanosheets can be act as the support and $Ag_2O$ nanoparticles are loaded homogenously on these nanosheets. In comparison to the TEM morphology of $Ag_2O$-$MnO_2$ material, an obvious difference is that the Ag nanoparticle size becomes small and the size distribution becomes narrower, the average size of Ag nanoparticles is about 5 nm for Ag-$MnO_2$ material (Fig. 2c). $Ag_2O$ nanoparticles are readily converted to Ag nanoparticles because of the reduction action of ethanol, and Ag nanoparticles are highly monodispersed on the $MnO_2$ nanosheets without agglomeration. The Ag nanoparticles are stably kept on the $MnO_2$ nanosheet surface, and this stability probably arises from the strong bonding interaction between the surface atoms of the nanoparticles and the surrounding oxygen atoms of the $MnO_2$ nanosheets. It is noteworthy that almost all of the Ag nanoparticles spatially correlate with the

nanosheets. In other words, there are no separated Ag nanoparticles under the condition of the confinement or support of $MnO_2$ nanosheets. The same reaction in the absence of manganese oxide nanosheets produces aggregated Ag nanoparticles (20-50 nm). It is very clear that $MnO_2$ nanosheets serve as effective nanoreactors for *in situ*

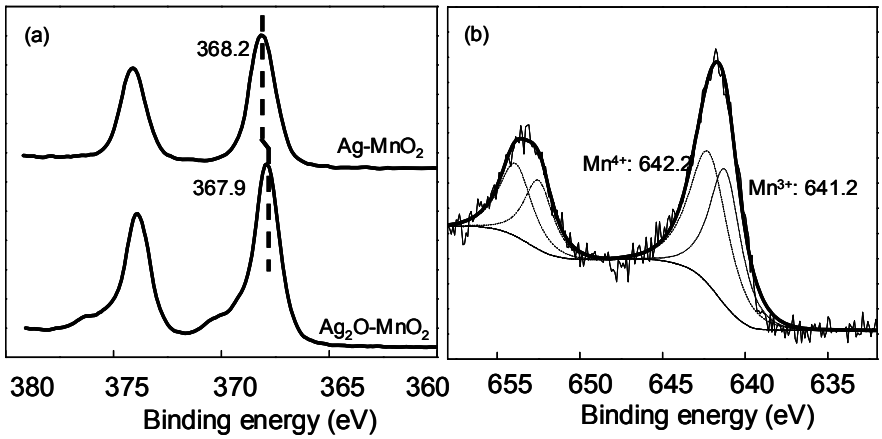


chemical transformation of monodispersed Ag nanocrystals without coagulation and bulk growth.

Fig.3 XPS spectra of $Ag_2O$-$MnO_2$ and Ag-$MnO_2$ materials: Ag 3d (a) and Mn 2p (b).

XPS provides a sensitive measure of the chemical state in the near surface region of material. It is carried out on the compounds to prove the reducibility of ethanol and identify the manganese oxide structure. The binding energy of the Ag $3d_{5/2}$ peak is about 367.9 eV in $Ag_2O$-$MnO_2$ material, suggesting that silver element exists in the form of $Ag^+$ ions.[33] A new peak at 368.2 eV can be observed for Ag-$MnO_2$ material, which can be assigned to Ag simple substance (Fig. 3a).[34] Therefore, it can be concluded that $Ag_2O$ can be reduced into silver perfectly in ethanol. The Mn 2p spectra of sample Ag-$MnO_2$ was individually divided by curve fitting to obtain the ionic state information of the element and to estimate the relative proportion of the different ionic states.[35] It can be seen that the sample shows two photoelectron peaks with different binding energies, indicating that there are two manganese sources. Two photoelectron peaks at 641.2 and 642.2 eV are ascribed to those of $Mn_2O_3$ and $MnO_2$, which are in good agreement with the literature (Fig. 3b).[36] On the basis of the peak areas, the average oxidation state of manganese is 3.56 in sample Ag-$MnO_2$. In comparison to the average oxidation state of manganese (3.67) reported by Post et al.,[37] it can be concluded that the content of $Mn^{III}$ is higher and the negative charge is more on $MnO_2$ nanosheets. Therefore, more $Ag^+$ ions can be absorbed and more Ag nanoparticles are loaded on $MnO_2$ nanosheets.

## 3.2. Electrochemical Behavior

CV is considered to be an ideal tool for the electrochemical property characterization and the specific capacitance calculation of the material. The electrochemical behavior of the obtained materials at different stages is investigated with a three-electrode cell and the results are shown in Fig. 4. For $MnO_2$ electrode material, the cyclic voltammetric curve is relatively rectangular in shape and exhibits a near mirror-image

current response on voltage reversal, indicating an obvious supercapacitive behavior. Meanwhile, the curve shows no obvious redox peaks, indicating that the electrode capacitor is charged and discharged at a pseudo-constant rate over the complete voltammetric cycle.[38,39] The specific capacitance value calculated from the CV curve is found to be 90 F $g^{-1}$ at 10 mV $s^{-1}$ in 1 mol $L^{-1}$ $Na_2SO_4$ electrolyte in the voltage from -0.05 to 0.95 V versus SCE. On the other hand, the cyclic voltammetry curves of $Ag_2O$-$MnO_2$ and Ag-$MnO_2$ electrodes are different from that of $MnO_2$ electrode under the same conditions. A pair of broad, symmetric, and well-separated redox peaks is observed, indicating that the measured capacitance is based on the redox mechanism. For $Ag_2O$-$MnO_2$ electrode, the cathodic peak is at 0.27 V and the anodic peak is at 0.58 V. In contrast, the Ag-$MnO_2$ electrode also shows a pair of well-defined redox peaks (anodic peak at 0.61 V, with corresponding cathodic peak at 0.19 V). The anodic and cathodic peaks shift respectively to the higher and lower potentials, pespectively, because of the lower electrode polarization of $Ag_2O$-$MnO_2$ electrode. In general, the reason of the electrode polarization is ascribed to the rate of the ion diffusion, electron transfer, and electrode reaction, but the rate for each process is not the same. For the Ag-$MnO_2$ electrode, the silver metal produced by the reaction helps to keep the internal resistance low and the electrical conductivity high as the cathode continues to discharge, and also, the specific capacitance and kinetic reversibility of the composite electrodes are significantly enhanced because of the addition of Ag nanoparticles. For the $Ag_2O$-$MnO_2$ electrode, the nanostructured $Ag_2O$ not only has the potential of high speed charge/discharge, but also promotes the redox reaction.[19] The specific capacitance of the $Ag_2O$-$MnO_2$ electrode is 232 F $g^{-1}$, while the specific capacitance is 272 F $g^{-1}$ for the Ag-$MnO_2$ electrode. In comparison to the specific capacitance of the $MnO_2$ electrode, $Ag_2O$-$MnO_2$ and Ag-$MnO_2$ electrodes show a larger specific

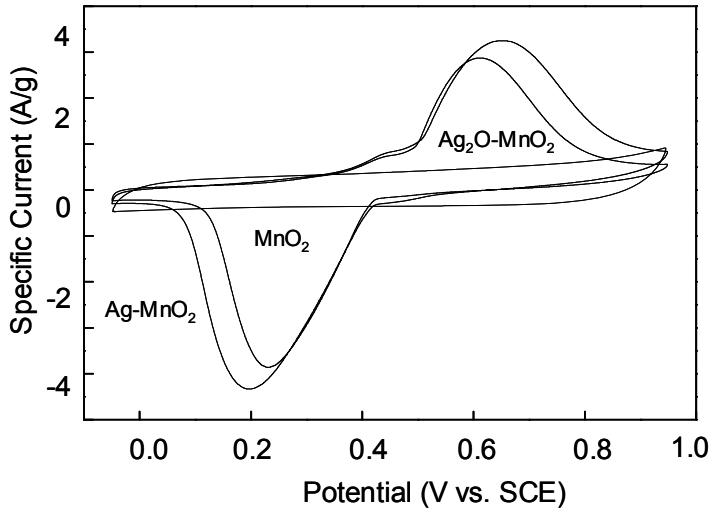


capacitance. The specific capacitance is 272 F $g^{-1}$ for the Ag-$MnO_2$ electrode. The larger specific capacitance is probably attributed to high electrical conductivity of $Ag_2O$-$MnO_2$ and Ag-$MnO_2$ electrodes, which facilitates the access of the electrolyte ions onto the $MnO_2$ surface and maximizes the use of manganese oxide pseudo-capacitance.[40]

Fig. 4. CV curves of pure $MnO_2$, $Ag_2O$-$MnO_2$, and Ag-$MnO_2$ materials at 10 mV $s^{-1}$ in 1 mol $L^{-1}$ $Na_2SO_4$ electrolyte in the voltage range -0.05–0.95 V vs. SCE.

CV curves of the Ag-$MnO_2$ electrode at different scan rates are shown in Fig. 5. At a scan rate of 5 mV $s^{-1}$, a broaden oxidation peak appears at 0.58 V and the corresponding reduction peak appears at 0.24 V. It can be noted that the oxidation peak shifts positively and the reduction peak shifts negatively with the increase of scan rates from 5 to 20 mV $s^{-1}$. It is well-known that the peak potential separation between the oxidation peak and the reduction peak is used as a measure of reversibility. The peak potential separation indicates that the Ag-$MnO_2$ electrode possesses worse

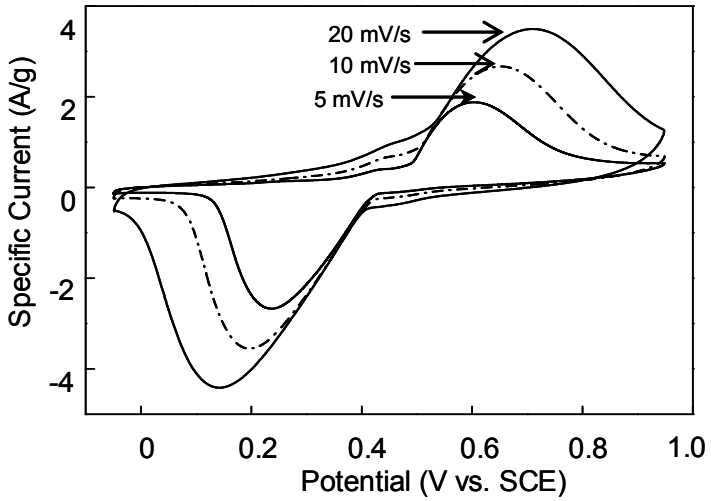


reaction reversibility with the increase of scan rates. The specific capacitance of Ag-$MnO_2$ electrode measured at 5, 10, and 20 mV $s^{-1}$ is 340, 272, 208 F $g^{-1}$, respectively. The decrease of capacitance ascribed to the effective use of the redox reaction is limited to some extent with the increase of the scan rate.[41]

Fig. 5. CV curves of the Ag-$MnO_2$ electrode at different scan rates in 1 mol $L^{-1}$ $Na_2SO_4$ electrolyte in the voltage range -0.05–0.95 V vs. SCE.

Electrochemical impedance can be used to understand the resistance characteristic. The Nyquist plots of pure $MnO_2$, $Ag_2O$-$MnO_2$, and Ag-$MnO_2$ materials are shown in Fig. 6. The Nyquist plots of the three cathode materials in 1 mol $L^{-1}$ $Na_2SO_4$ electrolyte are similar to each other in shape, consisting of a semicircle in the high frequency range and a straight line in the low frequency range. The semicircle at high frequency range is due to the charge transfer reaction at the interface of electrolyte/oxide electrode; it corresponds to the charge transfer resistance (Rct) and can be calculated by extrapolation of the semicircle on the real impedance axis.[42] From the Nyquist plots, the diameter of the semicircles decreases on the order of $MnO_2$ > $Ag_2O$-$MnO_2$ > Ag-$MnO_2$, indicating that Rct of the Ag-$MnO_2$ electrode is the smallest and the electrochemical reaction on the electrode/electrolyte interface is the most facile. This result confirms that the presence of silver nanoparticles indeed decreases the electronic resistivity of the electrode. In addition, the inclined line in the low frequency range is attributable to Warburg impedance, resulting from the frequency dependence of ion diffusion and transport in the electrolyte.[43] It can be seen that the linear region of the plot exhibits an angle relative to the real axis, and the angle relative to the real axis increases in the order of Ag-$MnO_2$ > $Ag_2O$-$MnO_2$ > $MnO_2$ electrode with the decrease of frequency. The large Warburg region for $MnO_2$ electrode indicates a great variation in the ion diffusion

path length and an increase of ion movement obstruction in the process of ion diffusion into the interior of the electrode.[44] Meanwhile, the value of the intercept at the real axis in the high frequency range can be used to estimate the solution or electrolyte resistance ($R_\Omega$), which is relevant to bulk electrolyte transport between the reference

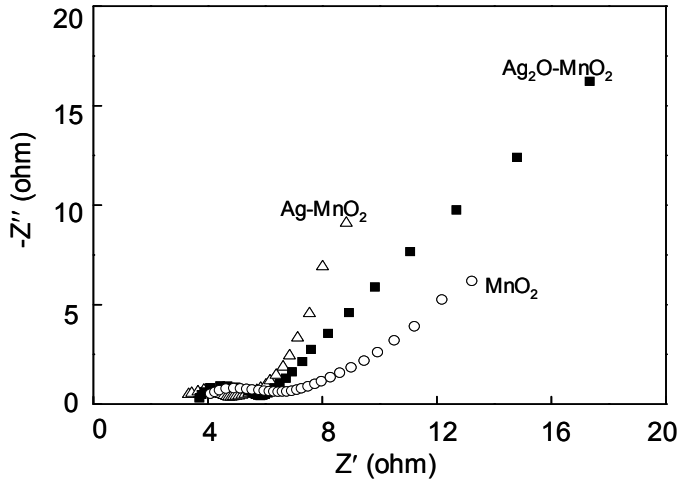


electrode and the working electrod. The resistance of $Ag_2O$-$MnO_2$ and Ag-$MnO_2$ electrodes is 3.7 and 3.3 Ω, respectively, which is lower than 4.1 Ω for the $MnO_2$ electrode. These results show that the Ag-loaded manganese oxide electrode can significantly improve the electrical performance because of the increase in conductivity.

Fig.6 Nyquist plots of pure $MnO_2$, $Ag_2O$-$MnO_2$, and Ag-$MnO_2$ electrode materials with a frequent range of 0.5 Hz to 8 $\times 10^4$ Hz in 1 mol $L^{-1}$ $Na_2SO_4$ electrolyte.

## 4. CONCLUSION

The Ag-loaded manganese oxide nanosheets (Ag-$MnO_2$) are prepared by chemically precipitating $Ag_2O$ nanoparticles on the surface of $MnO_2$ nanosheets, followed by a reduction reaction in a mixture solution of ethanol and PVP. Ag nanoparticles prevent the reassembling process of manganese oxide nanosheets, and Ag-$MnO_2$ electrode shows a characteristic Faradic capacitance behavior. This material takes not only full advantage of the pseudo-capacitance from manganese oxide but also the high electrical conductivity of silver nanoparticles. The Ag-$MnO_2$ material is a promising electrode one for an energy storage/conversion device with excellent performance.

**Acknowledgments** This work was supported by the National Natural Science Foundation of China (20971082 and 51172137), the Natural Science Key Foundation of Shaanxi Province (2011JZ001), the Changjiang Scholars and Innovative Research Team in University (IRT1070) and the Fundamental Research Funds for the Central Universities (GK200901002 and GK201001001).

## REFERENCES

1. Cheng, Q., Tang, J., Ma, J., Zhang, H., Shinya, N., Qin, L.-C. (2011), "Graphene and nanostructured $MnO_2$ composite electrodes for supercapacitors", *Carbon*, **49**(12), 2917-2925.

2. Hu, C.-C., Chang, K.-H., Lin, M.-C., Wu, Y.-T. (2006), “Design and tailoring of the nanotubular arrayed architecture of hydrous $RuO_2$ for next generation supercapacitors”, *Nano Lett.*, **6**(12), 2690-2695.
3. Simon, P., Gogotsi, Y. (2008), “Materials for electrochemical capacitors”, *Nat. Mater.,* **7**, 845-854.
4. Bordjiba, T., Bélanger, D. (2010), “Development of new nanocomposite based on nanosized-manganese oxide and carbon nanotubes for high performance electrochemical capacitors”, *Electrochim. Acta,* **55**(9), 3428-3433.
5. Roberts, A. J.; Slade, R. C. T. (2010), “Effect of specific surface area on capacitance in asymmetric carbon/$\alpha$-$MnO_2$ supercapacitors”, *Electrochim. Acta,* **55**, 7460-7469.
6. Staiti, P., Lufrano, F. (2009), “Study and optimisation of manganese oxide-based electrodes for electrochemical supercapacitors”, *J. Power Sources* **187**(1), 284-289.
7. Xue, T. Xu, C.-L., Zhao, D.-D., Li, X.-H., Li, H.-L. (2007)**,** “Electrodeposition of mesoporous manganese dioxide supercapacitor electrodes through self-assembled triblock copolymer templates”, *J. Power Sources*, **164**(2), 953-958.
8. Mathew, V., Lim, J., Kang, J., Gim, J., Rai, A. K., Kim, J. (2011), “Self-assembled mesoporous manganese oxide with high surface area by ambient temperature synthesis and its enhanced electrochemical properties”, *Electrochem. Commun.*, **13**(7), 730-733.
9. Zhang, W.-D., Chen, J. (2009), “Fabrication of a vertically aligned carbon nanotube electrode and its modification by nanostructured $MnO_2$ for supercapacitors”, *Pure Appl. Chem.*, **81**(12), 2317-2325.
10. Wei, W., Cui, X., Chen, W., Ivey, D. G. (2011), “Manganese oxide-based materials as electrochemical supercapacitor electrodes”, *Chem. Soc. Rev.*, **40**, 1697-1721.
11. Jeong, Y. U., Manthiram, A. (2002), “Nanocrystalline manganese oxides for electrochemical capacitors with neutral electrolytes”, *J. Electrochem. Soc.*, **149**(11), A1419-A1422.
12. Omomo, Y., Sasaki, T., Wang, L., Watanabe, M. (2003), “Redoxable nanosheet crystallites of $MnO_2$ derived via delamination of a layered manganese oxide”, *J. Am. Chem. Soc.*, **125**(12), 3568-3575.
13. Osada, M., Ebina, Y., Takada, K., Sasaki, T. (2006), “Gigantic magneto-optical effects in multilayer assemblies of two–dimensional titania nanosheets”, *Adv. Mater.*, **18**(3), 295-299.
14. Kaschak, D. M., Lean, J. T., Waraksa, C. C., Saupe, G. B., Usami, H., Mallouk, T. E. (1999), “Photoinduced energy and electron transfer reactions in lamellar polyanion/polycation thin films: Toward an inorganic “leaf””, *J. Am. Chem. Soc.*, **121**(14), 3435-3445.
15. Wu, X. M.; He, Z. Q.; Chen, S.; Ma, M. Y.; Xiao, Z. B.; Liu, J. B. Silver-doped lithium manganese oxide thin films prepared by solution deposition. *Mater. Lett.* 2006, **60**(20), 2497-2500.
16. Ahn, H.-J., Sung, Y.-E., Kim, W. B., Seong, T.-Y. (2008), “Crystalline Ag nanocluster-incorporated $RuO_2$ as an electrode material for thin-film micropseudocapacitors”, *Electrochem. Solid-State Lett.*, **11**(7), A112-A115.
17. Wang, Y., Zhitomirsky, I. (2011), “Cathodic electrodeposition of Ag-doped manganese dioxide films for electrodes of electrochemical supercapacitors”, *Mater. Lett.*, **65**(12), 1759-1761.

18. Wang, S., Xie, J., Zhang, T., Varadan, V. K. (2009), “Silver decorated γ-manganese dioxide nanorods for alkaline battery cathode”, *J. Power Sources*, **186**(2), 532-538.
19. Pan, J., Sun, Y., Wang, Z., Wan, P., Liu, X., Fan, M. (2007), “Nano silver oxide (AgO) as a super high charge/discharge rate cathode material for rechargeable alkaline batteries”, *J. Mater. Chem.*, **19**(17), 4820-4825.
20. Linden, D., Reddy, T. B. (2002), *Handbook of Batteries,* 3rd ed.; McGraw-H: New York,; pp 12.1-12.17.
21. Pistoia, G. (2009), “*Battery operated devices and systems: from portable electronics to industrial products”*; Elsevier: Amsterdam, The Netherlands; pp 24-25.
22. Feng, Q., Liu, L., Yanagisawa, K. (2000), “Effects of synthesis parameters on the formation of birnessite-type manganese oxides”, *J. Mater. Sci. Lett.*, **19**(17), 1567-1570.
23. Liu, Z.-H., Yang, X., Makita, Y., Ooi, K. (2002), “Preparation of a polycation-intercalated layered manganese oxide nanocomposite by a delamination/reassembling process”, *Chem. Mater.*, **14**(11), 4800-4806.
24. Yan, J., Wei, T., Qiao, W., Shao, B., Zhao, Q., Zhang, L., Fan, Z. (2010), “Rapid microwave-assisted synthesis of graphene nanosheet/$Co_3O_4$ composite for supercapacitors”, *Electrochim. Acta*, **55**(23), 6973-6978.
25. Yuan, C.-Z., Gao, B., Zhang, X.-G. (2007), “Electrochemical capacitance of NiO/$Ru_{0.35}V_{0.65}O_2$ asymmetric electrochemical capacitor”, *J. Power Sources*, **173**(1), 606-612.
26. Yuan, J., Liu, Z-H., Qiao, S., Ma, X., Xu, N. (2009), “Fabrication of $MnO_2$-pillared layered manganese oxide through an exfoliation/reassembling and oxidation process”, *J. Power Sources*, **189**, 1278-1283.
27. Sasaki, T., Watanabe, M. (1998), “Osmotic swelling to exfoliation. Exceptionally high degrees of hydration of a layered titanate”, *J. Am. Chem. Soc.*, **120**(19), 4682-4689.
28. Ni, P., Li, H., Yang, M., He, X., Li, Y., Liu, Z.-H. (2010), “Study on the assembling reaction of graphite oxide nanosheets and polycations”, *Carbon*, **48**(7), 2100-2105.
29. Zhou, Q., Zhang, C., Liu, Z.-H., Tang, X., Li, H. (2007), “Preparation of lysine-intercalated manganese oxide nanocomposite by a delamination/reassembling process”, *Colloids Surf. A*, **295**, 269-273.
30. Li, B., Cao, H., Shao, J., Li, G., Qu, M,, Yin. G. (2011), “$Co_3O_4$@graphene composites as anode materials for high-performance lithium ion batteries”, *Inorg. Chem.*, **50**(5)*,* 1628-1632.
31. Xu, C., Wang, X., Yang, L., Wu, Y. (2009), “Fabrication of a graphene-cuprous oxide composite”, *J. Solid State Chem.*, **182**(9)*,* 2486-2490.
32. Gao, Q., Giraldo, O., Tong, W., Suib, S. L. (2001), “Preparation of nanometer-sized manganese oxides by intercalation of organic ammonium ions in synthetic birnessite OL-1”. *Chem. Mater.*, **13**(3), 778-786.
33. Kaspar, T. C., Droubay, T., Chambers, S. A., Bagus, P. S. (2010), “Spectroscopic evidence for Ag(III) in highly oxidized silver films by X-ray photoelectron spectroscopy”, *J. Phys. Chem. C*, **114**(49), 21562-21571.
34. Murray, B. J., Li, Q., Newberg, J. T., Menke, E. J., Hemminger, J. C., Penner, R. M. (2005), “Shape- and size-selective electrochemical synthesis of dispersed silver(I) oxide colloids”, *Nano Lett.*, **5**(11), 2319-2324.

35. Hermas, A. A. (2008), “XPS analysis of the passive film formed on austenitic stainless steel coated with conductive polymer”, *Corros. Sci.*, **50**(9), 2498-2505.
36. Reddy, A. S., Gopinath, C. S., Chilukuri, S. (2006), “Selective *ortho*-methylation of phenol with methanol over copper manganese mixed-oxide spinel catalysts”, *J. Catal.*, **243**(2), 278-291.
37. Post, J. E., Heaney, P. J., Hanson, J. (2002), “Rietveld refinement of a triclinic structure for synthetic Na-birnessite using synchrotron powder diffraction data”, *Powder Diffr.*, **17**(03), 218.
38. Bao, S.-J., He, B.-L., Liang, Y.-Y., Zhou, W.-J., Li, H.-L. (2005), “Synthesis and electrochemical characterization of amorphous $MnO_2$ for electrochemical capacitor”, *J. Power Sources*, **132**(1-2), 315-320.
39. Xu, M., Kong, L., Zhou, W., Li, H. (2007), “Hydrothermal synthesis and pseudocapacitance properties of $\alpha$-$MnO_2$ hollow spheres and hollow urchins”, *J. Phys. Chem. C*, **111**(51), 19141-19147.
40. Hou, Y.; Cheng, Y.; Hobson, T.; Liu, J. (2010), “Design and synthesis of hierarchical $MnO_2$ nanospheres/carbon nanotubes/conducting polymer ternary composite for high performance electrochemical electrodes”, *Nano Lett.*, **10**(7), 2727-2733.
41. Qu, Q.; Zhang, P.; Wang, B.; Chen, Y.; Tian, S.; Wu, Y.; Holze, R. (2009), “Electrochemical performance of $MnO_2$ nanorods in neutral aqueous electrolytes as a cathode for asymmetric supercapacitors”, *J. Phys. Chem. C*, **113**(31), 14020-14027.
42. Ghaemi, M., Makhlooghi, F., Adelkhani, H., Aghazadeh, M., Shiri, H. M. (2010), “The influence of electroless silver deposition on electrochemical properties of the steel cathode current collector of alkaline batteries”, *Int. J. Electrochem. Sci.*, **5**, 131-146.
43. Du, X.; Guo, P.; Song, H.; Chen, X. (2010), “Graphene nanosheets as electrode material for electric double-layer capacitors”, *Electrochim. Acta*, **55**(16), 4812-4819.
44. Stoller, M. D., Park, S., Zhu, Y., An, J., Ruoff, R. S. (2008), “Graphene-based ultracapacitors”, *Nano Lett.*, **8**(10), 3498-3502.